Versatile Selective Absorption-Based Optical Fiber toward Epinephrine Detection

Tahereh Azargoshasb[1], Roghaieh Parvizi[2, *], H. Ali Navid[1, *], Gholam-Mohammad Parsanasab[3], and Hadi Heidari[4]

[1]*Department of Laser and Optical Engineering, University of Bonab, Bonab 5551761167, Iran*
[2]*Department of Physics, College of Sciences, Yasouj University, Yasouj 75914-353, Iran*
[3]*Integrated Photonics Laboratory, Faculty of Electrical Engineering, Shahid Beheshti University, Tehran, Iran*
[4]*James Watt School of Engineering, University of Glasgow, Glasgow, G12 8QQ, United Kingdom*

Abstract - A versatile lossy mode resonance (LMR) sensor is developed for Epinephrine monitoring based on the state-of-the-art molecular imprinting technique over an optical fiber. The optical absorption concept of the LMR-based sensor is proven by incorporating an amino silane-functionalized graphene oxide (SiO_2-NH_2@GO) as an adhesive layer for grafting Epinephrine imprinting polydopamine (Ep-IPDA) as a sensing layer onto the optical fiber curved surface. The accurate structural and morphological characterization confirmed the rough crystalline and spherical particles for Ep-IPDA and SiO_2-NH_2-GO onto optical fiber curved surface, while spectroscopic analysis confirms the formation of imprinting polymer and desirable absorbance characteristics. The optimized probe exhibits an excellent performance with the maximum sensitivity within two intervals of 0.3-1 µM and 1-90 µM along with the linearity coefficient of R^2= 0.99 possessing a low limit of detection of 0.07 µM. Additionally, this sensor selectively detects Ep in the presence of other species and showed good recovery in human urine and injection samples. This work opens a new avenue for developing bio-inspired LMR-based optical fiber biosensors and could be further extended to detect other catecholamine neurotransmitters.

Keywords: Lossy Mode Resonance, Optical Fiber Biosensors, Molecular Imprinting Polymer, Epinephrine, Polydopamine, Graphene Oxide.

1. Introduction

Epinephrine (Ep), a vital catecholamine neurotransmitter released by the adrenal glands, plays an essential role in the human nervous system [1]. It is responsible for several life phenomena such as exciting the heart muscle, increasing blood pressure, and rapid relieving signs [2]. Many diseases are related to the variation of Ep concentration in blood levels [3]. Therefore, quick and precise quantification of Ep in human fluids such as plasma and urine is of exceptional importance in medical diagnostics, especially for patients with 'Parkinson's disease, pheochromocytoma, and stress [1, 4, 5]. Although many traditional techniques such as capillary electrophoresis [6], fluorescence [7], chemiluminescence [8], high-performance liquid chromatography [9], Colorimetric [10], and electrochemical methods [11-14] are used to detect Ep, these strategies raise several issues related to complexity, cost, and time-consuming.

Light transmission through optical waveguides has been a topic of interest in modern optical-analytical chemistry due to its extreme specificities. This field of study is evolving in clinical diagnostics [15, 16], therapeutic monitoring, organism detection [17, 18], and toxins [19]. With the development of optical sensors, it is possible to utilize fiber-based sensors due to their portable and miniaturized design, simplicity, biocompatibility, high sensitivity, wide bandwidth, and immunity to electromagnetic interferences [20, 21]. The most striking feature of these platforms is interacting with biological substances through the utilization of sensitive absorbing layers to modulate the characteristics of light, known as absorption-based Lossy Mode Resonance (LMR) optical sensors [22, 23]. In LMR, the coupling between a waveguide mode and a specific lossy mode of a thin film occurs at a film thickness according to the overlap of mode fields and phase-matching conditions. The phase-matching condition requires equality of the real part of lossy and waveguide modes' propagation constants [24]. A similar phenomenon, surface plasmon resonance (SPR), occurs on the dielectric-metal interface when the guiding mode couples to surface plasmon polariton mode under phase-matching conditions. Although a lot of reported literature has been devoted to the SPR, the number of publications debating LMR is still relatively low. While LMR sensors can be excited by both TE (transverse electric) and TM (transverse magnetic) polarization modes, SPR occurs with TM polarized light. Therefore, the experimental setup of optical devices is simplified to a great extent with LMRs.

Besides, SPRs are typically found for angles ranging between 40° and 70° in a Kretsch Mann configuration [25], whereas LMRs stem from typically near-grazing angle incidence. In this respect, LMR-based sensors can be better merged with optical fibers. Also, LMR-based sensors can generate multiple attenuation dips in the transmittance spectra by increasing the coating material thickness. So, the sensitivity of the as-prepared sensor can be tuned just by changing the thickness of the thin film layer, which is not possible for SPR-based sensors. It is shown that the sensitivity of the LMR-based sensors is significantly higher than that of the SPR sensors[26].

In recent years, a combined approach of sensors and molecular imprinting polymer (MIP) has been applied to fabricate a sensor to address specificity by only interacting the sensing interface with the analyte to select a particular analyte. Furthermore, numerous studies have reported on the integration of the merits of MIP and its sensor templates in the last decades, such as biological molecules, inorganic ions, drugs, nucleic acids, proteins, viruses, and even cells [27]. However, it is not always possible to apply MIPs, due to the low stability and reactivity, resulting in low sensitivity and mass accumulation. There is a particular focus on the limitations of methods to produce hydrophobic polydopamine based MIP on fiber at low temperatures with strong silane/graphene oxide GO) based interfacial adhesion [28, 29].

This work focuses on the design and fabricating of a versatile Ep fiber-based sensor by in situ coating of a polydopamine (PDA)-based molecularly imprinted film grafted over aminosilane-functionalized graphene oxide (Ep-IPDA). The PDA-grafted graphene oxide enables selective binding to a specific analyte based on a unique optical absorption characteristic. Due to the oxygen-enriched functional groups such as carboxyl, hydroxyl, and epoxide groups, GO has become an invaluable nanomaterial for polymer coating reinforcement [30]. Moreover, SiO_2-NH_2@GO coupling agents have been extensively applied to impart distinctive properties to GO. Since the silane coupling agents form chemical bonds with molecules containing functional groups of GO and organic polymers, this leads to different properties depending on their nature. These properties represent improved water resistance, interfacial adhesion, and optical and electrical properties that have been optimized as an LMR fiber-based optical sensor. Overall, this sensor

benefited from integrating an optical fiber with the PDA-grafted SiO_2-NH_2@GO and showed excellent reproducibility and sensitivity with a low limit of detection (LOD) of only 0.07 µM for fast Ep detection.

2. Preparation of PDA@SiO_2-NH_2@GO coated probe

The strategy to fabricate sensing probes initially involves the clad removing and treating polymer-clad silica (PCS) multi-mode fiber with a 200 µm core diameter and numerical aperture of 0.39. The etching rate and cleaning of the clad removed optical fiber are explained as well as the illustration of the spectra. Afterward, *in situ* fabrication of improved interface structures on optical fibers is followed by two coating stages, firstly SiO_2-NH_2@GO and then self-polymerized PDA with imprinted Ep analytes. The amount of 0.01 g of GO is dispersed in 10 mL Ethylene glycol through ultrasonication for 1 h; 1 mL TEOS and 0.4 mL APTES and 10 mL Methanol were added, and the mixture is stirred vigorously for 0.5 h to prepare the silane solution at room temperature using Sol-gel method. The pH of the silane mixture is adjusted at 5-6 by hydrochloric acid accompanied by adding 3 drops of Glycine solution mixed to prevent the agglomeration, followed by 15 min mixing. In the hydrolysis process of TEOS (HTEOS), silica is loaded on a GO sheet surface with covalent bonds (as shown in Fig. 1(a)) as hydroxyl groups of HTEOS can interact with the carboxylic groups at the GO edges. APTES agent also can be applied to catalyze inter- or intra-molecularly the reaction between TEOS molecules as grafted on GO surface through the hydrogen bonding. The linkages of silane molecules with terminal epoxide with amine groups of the hardener lead to a much more robust network.

In the following, the polydopamine is coated on the surface of the SiO_2-NH_2@GO coated optical fiber using the simple solution oxidation polymerization method without complicated instruments. A solution of DA (0.1g to 20 mL buffer tris pH 8.5, 0.1 M) was prepared and then 5 mL of 100 ppm Ep solution was added to the previous solution. After that, optical fibers were put in this solution. Then, the SiO_2-NH_2@GO coated optical fiber was exposed to a solution of polydopamine at various times of 6, 8, and 12 h at ambient conditions. Due to slow and moderate reaction rates, tris buffer (pH 8.5) can be exploited to efficiently control PDA morphology and film thickness [31]. DA is oxidized in a high-pH solution and dark environment, providing its quinone derivative, and then the reaction will proceed to self-polymerize to

generate polydopamine. Dopamine-quinine, as the intermediate step, could be manipulated by the nucleophiles in the Tris buffer, hindering the particle growth, and giving rise to the PDA particles with a much smaller average size. Finally, to get the MIP layer, the template molecules were removed from the imprinted polymer layer by immersing the probe in methanol and acetic acid (9:1) for a required time and the washing process was explained in the supplementary text. The washing time was determined by repeating the cycle sensing measurements for each probe washed at different times. To obtain a suitable wash time, first, the probe was immersed in a solution of methanol and acetic acid for 30 minutes. The output signal of the probe was recorded, then the process was repeated up to 7 times, and the best performance was 2.5 hours of immersing. The experimental setup applied for the sensor probe characterization is shown in Fig1. (b), both ends of the fiber-probe were cleaved and cleaned using Isopropyl alcohol, ensuring the maximum light coupling into the fiber.

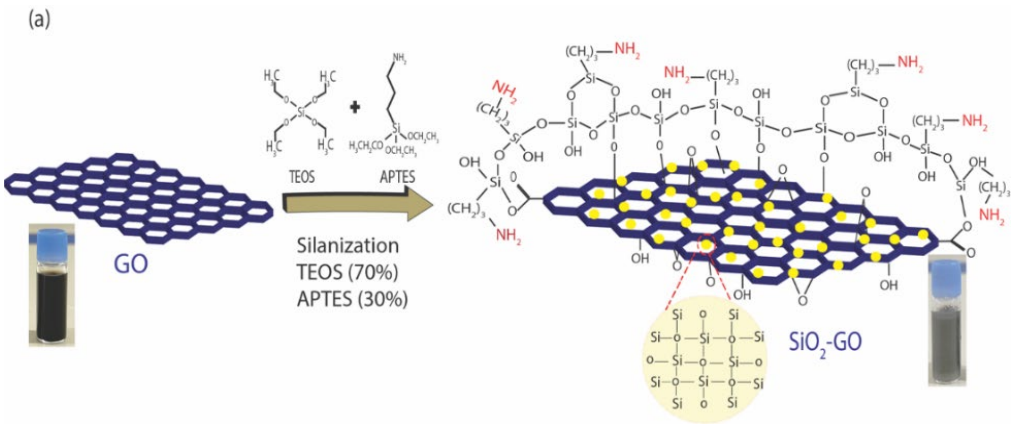

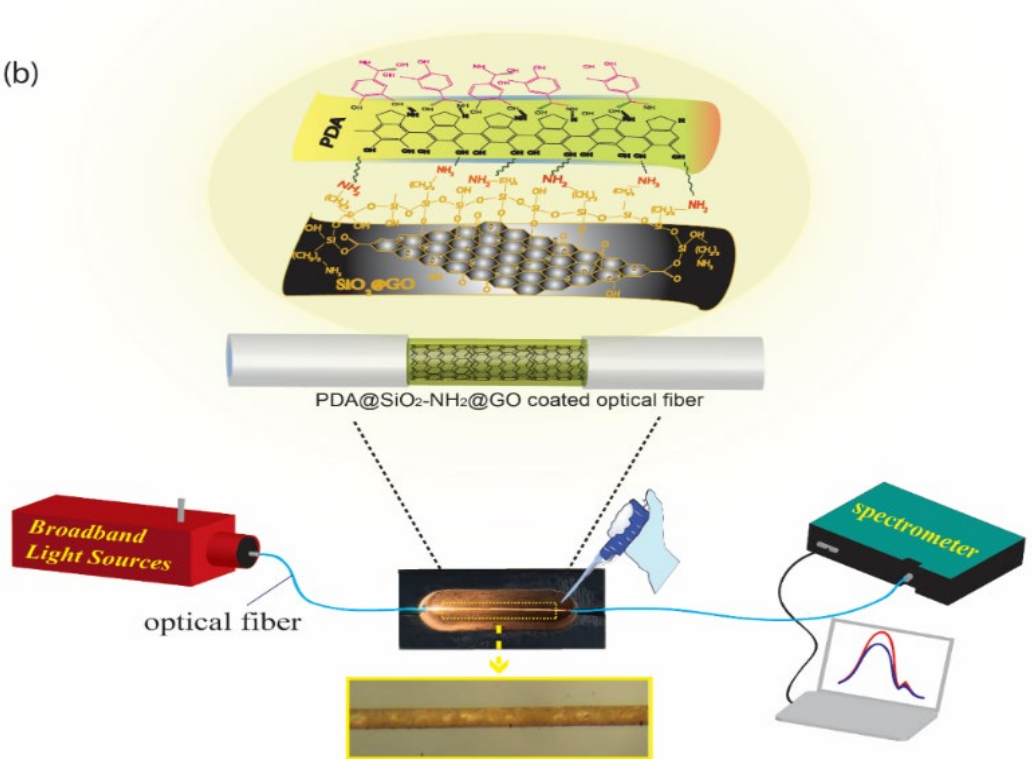

Fig.1: (a) Chemistry of polymerization of Ep-IPDA before EP removal. **(b)** Diagram of the experimental setup and the configuration of fiber optic probes and image of coated optical fiber.

3. Results and discussion:

3.1 Characterization

FTIR analysis is conducted to investigate the surface chemical structure of SiO_2-NH_2@GO, PDA, and Ep-IPDA before and after removing Ep (see Fig. 2). For SiO_2-NH_2@GO powder, peaks appeared at 3411, 1124, 934, and 565 cm^{-1} represent the bending and asymmetric vibrations of OH, Si-O-C, Si-OH, and Si-O-Si bonds, respectively [32-34]. Moreover, peaks determined at 1124, 804, and 472 cm^{-1} are assigned to the asymmetric, symmetric, and bending vibration of the Si-O-Si bond, respectively. It can be seen that the peaks related to the Si-O-Si bond are the most intensive ones among the other peaks, displaying that silane is essentially deposited on the GO surface forming SiO_2-NH_2@GO composite. The shoulders that emerged at 2934 and 2872 cm^{-1} can be related to the stretching vibrations of –CH3 stretching vibrations and amino (NH_2) functional groups denoting the presence of APTES on the GO surface [33]. The appeared shoulder

besides, at 1737 cm^{-1} regarding C=O stretching vibration indicates that TEOS and APTES reduced the GO through covalent functionalization with the carboxylic groups at the edges of GO. Also, peaks at 2923 can be attributed to –CH_3 stretching vibrations. In the spectrum of Ep-IPDA, the peaks at 1500 and intervals of 3400 cm^{-1} correspond to the benzene groups and OH stretching vibration, respectively. Generally, all the spectra (shown in Fig. 2(a) and Fig. S2(a) regarding the DA and Ep) reveal a peak at 1511 corresponding to the shearing vibration of N–H in the amide group, which is mainly responsible for grafting the whole structure.

The XRD pattern of SiO_2-NH_2@GO composites (Fig 2(b)) shows a broad intensive diffraction peak around 2 θ=22° that is ascribed to the diffraction of SiO_2 nanoparticles [35]. It can be seen from XRD patterns that silane deposition on the GO surface significantly weakened the characteristic diffraction peak of GO. The rest of Fig. 2(b) presents the XRD patterns of the PDA, and Ep-IPDA before and after removing Ep, respectively. As it can be observed, the broad reflection peak ascertains the similar amorphous nature of MIP-PDA before and after removing Ep [36]. Fig. 2(g) implies the existence and well dispersed of Ep within the PDA@SiO_2-NH_2@GO as the phase is formed according to the XRD pattern of Ep structure (shown in Fig. 2(g) dashed line). Additionally, comparing Figs. 2(g) and 2(h) represent well removal of Ep within the PDA@SiO_2-NH_2@GO removed Ep solution [13].

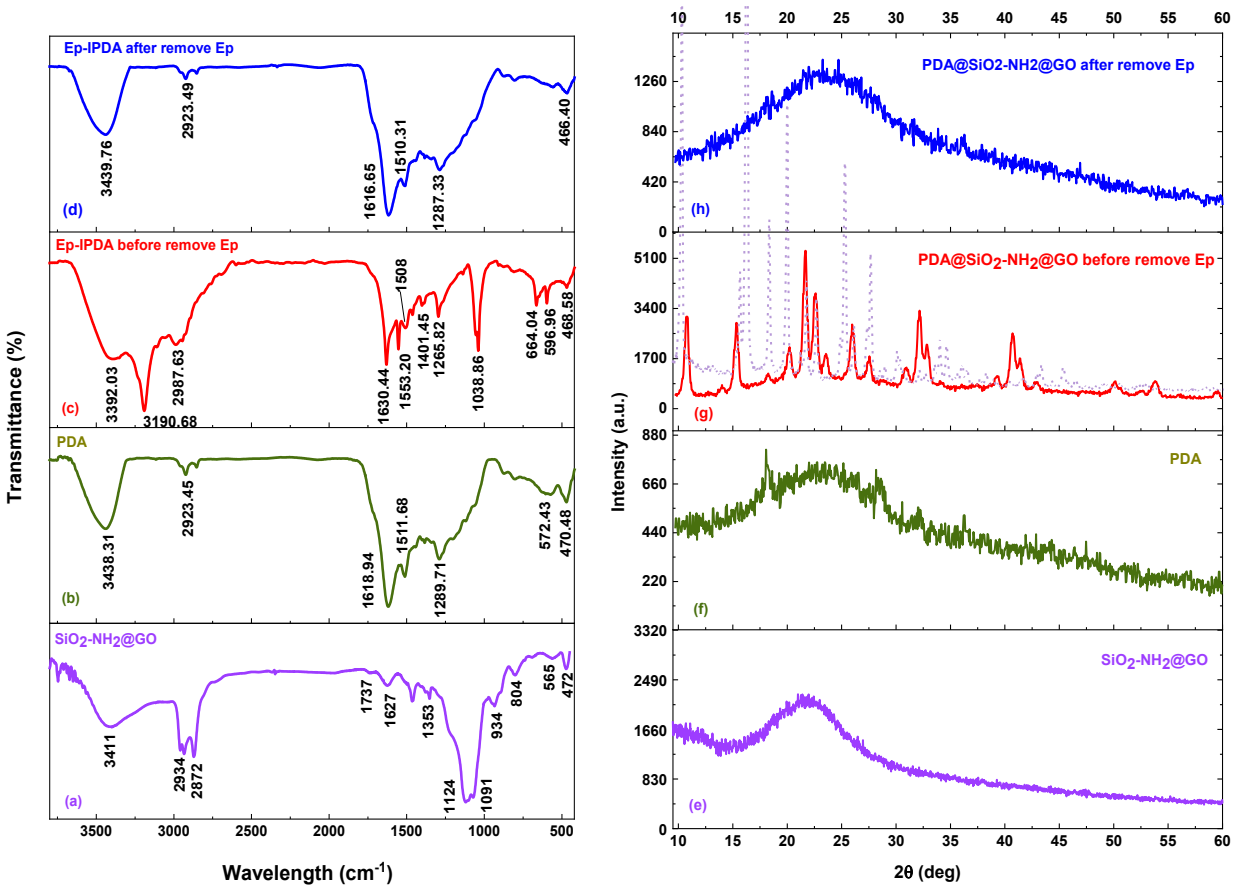

Fig. 2: FTIR spectra and XRD pattern of (a, e) SiO_2-NH_2@GO, (b, f) PDA, (c, g) Ep-IPDA before removing Ep and (d, h) Ep-IPDA after removing Ep, respectively.

The FE-SEM images of GO and SiO_2-NH_2@GO sheets are shown in Fig. 3. The pristine GO sheets with tightly stacked structure layers [Fig. 3 (a)], and the morphology and size of SiO_2 nano-particles covered the GO layers (carboxylic at edges and epoxide in the basal plane introducing the silane functionalized GO), preventing the re-stacking of GO sheets during the drying stage. The size range of spherical particles is less than 100 nm, while there is some agglomeration (larger than 200 nm in diameter). Based on these explanations, the pristine GO sheets are successfully covered with silica nano-particles (which was previously proved by Fourier-transform infrared spectroscopy (FT-IR) analysis). Also, Fig. 3(b) illustrates that in this composite without PDA coating, most of the SiO_2 nano-particles agglomerate together.

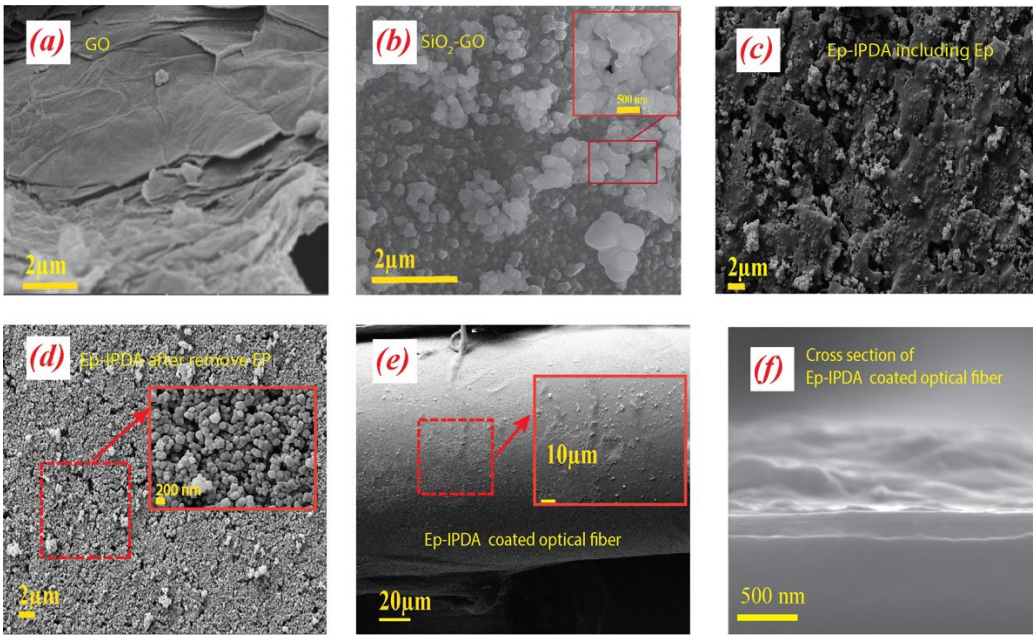

Fig. 3: FE-SEM image of (a) GO, (b) SiO_2-GO, (c) Ep-IPDA before EP removal, (d) Ep-IPDA after removing Ep, (e) Ep-IPDA after removing Ep coated optical fiber and (f) cross-section of Ep-IPDA after removing Ep.

After polymerization of DA, including template molecule of Ep, through self-polymerization route identified as MIP, FE-SEM image (Fig. 3(c)) shows the surface of SiO_2-NH_2@GO coated optical fiber is thoroughly covered by PDA layers, which is significantly different from the original SiO_2-NH_2@GO. Therefore, it indicates the successful synthesis of uniformly anchored PDA on the surface of SiO_2-NH_2@GO coated optical fiber. Also, comparing this SEM image with the Ep molecules-removed sample, an appreciable homogeneous coating with well-dispersed particle size ranges from nearly 50 to 150 nm occurred, which may be caused by the PDA-coating layer. It implies that GO sheets are well wrapped up on the SiO_2 particles and well dispersed in sample Ep-IPDA, Fig. 3(d). The washing and removal of the template molecule, the polymerization process revealed that PDA could effectively prevent the agglomeration of SiO_2 particles and lead to a uniform distribution of imprinted sites in the polymer shown in Fig.3 (e, with the magnified image in 10 µm scale, and f), that provides a versatile sensing platform. Indeed, the uniform distribution of imprinted sites in the polymer decides the efficiency of sensing

performance, which has been cared for in any steps. According to the SEM image in Fig. 3(f), the thickness of the optimized as-prepared probe cross-section is 360nm.

A UV−Vis spectrometer evaluated the optical characteristics of the Ep-IPDA solution. The encapsulated nanoparticles could absorb visible light upon PDA deposition, which resulted from PDA optical absorption of visible light, especially by the green color region, Fig. 4(a). The as-prepared Ep-IPDA in an aqueous solution exhibit an intense emission with a maximum of about 470 nm. The direct Tauc plot evaluated for this spectrum also verifies a bandgap of 2.25 eV corresponding to the absorption wavelength of more than 551 nm [37]. Similarly, visible light absorption could be seen in the obtained spectra using Differential reflectance spectroscopy (DRS), implying the trace of Ep molecules presence clearly by the emergence of less absorption within the starting visible region (around 500 nm). This can directly introduce this composite as an efficient and versatile sensing layer to trap and detect Ep molecules.

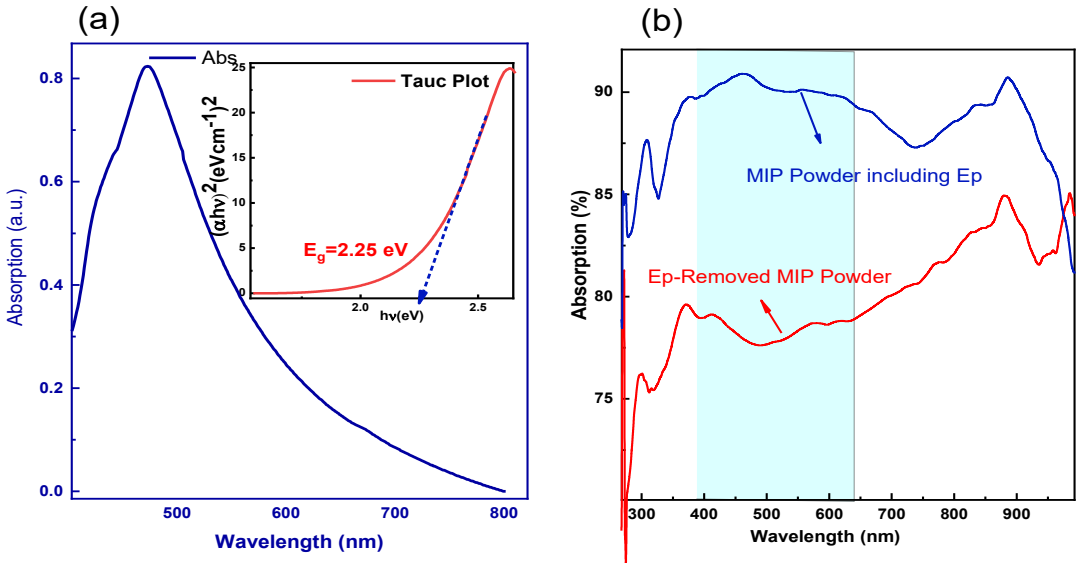

Fig. 4: (a) UV–VIS absorption spectra and (b) DRS spectral of Ep-IPDA after removing Ep.

3.2 Sensing characterization

SiO_2-NH_2@GO coated optical fiber performance:

As explained in section 2, there are two tasks to complete the Ep optical sensing probe fabrication. Firstly, the GO is coated on optical fibers using a silane sol-gel process to examine the possibility of GO-coating

as an absorbent layer on the curved glass surface of optical fiber, and also to assess the effect of various GO concentrations. Secondly, the self-polymerized Ep-IPDA-coated optical fiber is studied under different polymerization times to test the sensing performance. Accordingly, the optimal treatment conditions of GO grafting are investigated using four concentrations of 0.001, 0.005, 0.01, and 0.1g of GO-incorporated silane. The optical fiber probes are exposed to the surrounding refractive index (RI), and the corresponding transmitted spectra are recorded (as shown in Fig. S3). The obtained results revealed that owing to the low RI contrast between silica and SiO_2-NH_2@GO layer, the transmission spectrum is minimally affected by probes with SiO_2-NH_2@GO coatings using GO concentration of 0.001g. Due to more GO concentrations of 0.005 and 0.01g at the coated SiO_2-NH_2@GO layer, a reasonable RI sensitivity could be expected, mainly attributable to the weak absorption.

Ep-IPDA-coated optical fiber performance:

To establish the Ep-IPDA-coated optical fiber, dopamine is used to functionalize the SiO_2@GO hybrids. The PDA shell on the surface of Ep-IPDA improves the interfacial adhesion between the nano-hybrids and simplifies the homogeneous dispersion of SiO_2@GO onto the optical fiber. The covalent and the hydrogen bonding interactions between PDA and the GO sheets can strongly immobilize the Si nano-particles on the GO sheet. This mainly occurred due to hydrogen bonding between the amino groups ($-NH_2$) of APTES and PDA [38], as shown in SEM images in Fig. 3(e). Moreover, the PDA coating introduces chemical groups and enhances the surface reactivity and polarity to trap the Ep targets. As a result, the Ep conformal and continuous detection is evaluated using an optical probe to validate a versatile Ep formation of the solid template through oxidation, cyclization, and polymerization reactions. Primarily, the optimized concentration of GO is determined, and the polymerization process of PDA is investigated. The probe is tested for different concentrations of Ep ranging from 0.1 μM and 140 μM, and different RI and the shift in resonance wavelength are extracted from the LMR spectra. The experiments are repeated 4-5 times, and the average resonance wavelength is determined for each concentration, with the calculated standard deviation displayed as error bars for each concentration. The calibration curves for Ep determination are

obtained using successive addition of an aqueous stock solution (elution of the composite with Methanol/deionized-water mixture). The obtained results depicted in Fig.S5 reveal that although samples prepared with 3h silane exposure time can provide sensitivity to Ep, they cannot render a wide range of sufficient absorption - and consequently, LMR-based sensitivity performance - even if the PDA exposing time increases to 6 and 12h. This matter is shown in Figs. 5(c), 5(d) and Fig.S5. In the case of 12h polymerization, the shift is not considerable, and only the intensity variation versus Ep is obtained due to the nature of the evanescent wave.

The probe is treated by immersing it into SiO_2-NH_2@GO solution for 5h and then in polymerized PDA for 6h with the 0.01g of GO. Then, it is characterized using Ep with concentrations ranging from 0.3 to 70μM. The LMR spectrum is recorded for each concentration. Fig. 5(a) shows a decrease in dip wavelength with increasing Ep concentration. This could be attributed to the imaginary part decrement of the sensing layer effective RI. The resonance wavelength extracted from each LMR spectra is illustrated in Fig. 5(b) as a function of Ep concentration. In Figs. 5(c) and 5(d), the probe is treated by placing it into GO@SiO_2-NH_2 solution for 3h and then in polymerized PDA for 8h with the finalizing parameter of 0.01g of GO. Again, it is characterized using Ep concentrations ranging from 0.3 to 60μM, and the LMR spectra are recorded for each concentration. The recorded results are linear within two intervals of 0.3-1μM and 1-50μM with a slope of 9.554nm/μM and 0.086nm/μM, respectively. Also, the correlation efficiencies (R^2) are 0.96 and 0.993, respectively. It can be observed that this layer does not result in a sufficient number of surface imprinted sites, which directly affects the sensor sensitivity. At the same time, an excess of deposition time may result in a suitable sensing thickness, which decides the Ep detection by PDA molecular imprinting performance, and provides an efficient specific analyte monitoring.

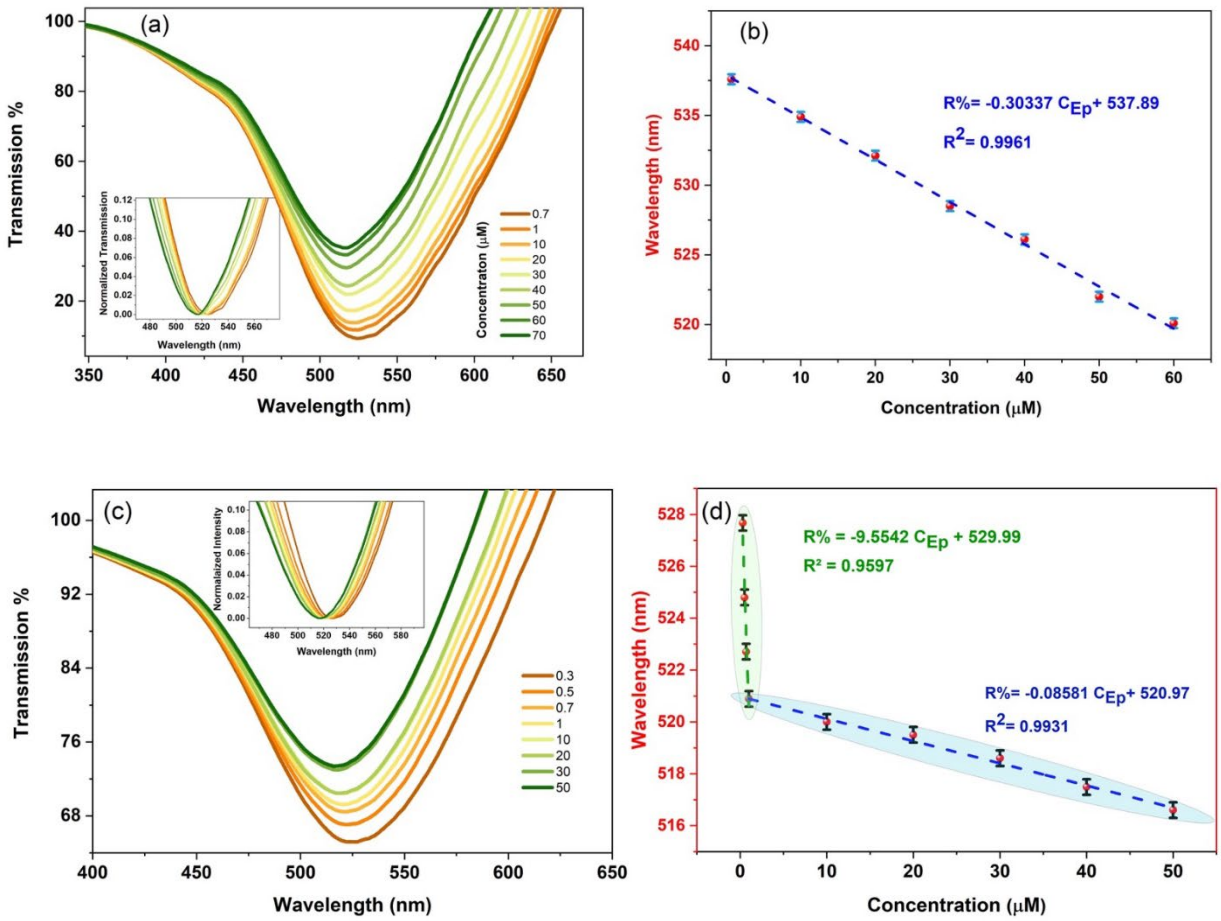

Fig. 5: (a) LMR spectra, and (b) variation of resonance wavelength with Ep concentration in 5h silane Sol-gel step and 6h PDA polymerization. (c and d) LMR spectra and variation of resonance wavelength with epinephrine concentration in 3h silane Sol-gel step and 8h PDA polymerization.

The exposing time of the probe in solution and PDA deposition decide the thickness of the layer. An FE-SEM image of the PDA deposition on optical fiber is shown in Fig. S7. The residual thickness has an important influence on the mode interference in the fiber [39]. So, this parameter directly affects the efficiency of the LMR-based optical fiber sensor [40]. For this matter, the different exposing times are also considered as 5h, 8h and 12h for depositing PDA onto the SiO_2-NH_2@GO coated optical fiber. It is observed that for the sample with exposing time of 8h, a maximum shift of 27nm in resonance wavelength is obtained for 300nM to 90μM, shown in Fig. 6(a). In this way, two linear intervals appear in the sensitivity diagram. The number of surface sites available per Ep molecule decreases with prolonged deposition time,

and more light modes could be absorbed within the sensing layer before reaching the surface. In general, tracking the LMR shift in the transmission spectrum is the basis of Ep detection. It is well known that some physical phenomena, such as inter-particle coupling, change in particle size or shape, charging of particles, and change in electron dynamics can change the resonance wavelength position. Blue shifts can usually be attributed to the lowering of particle size or excess electrons on the particle due to charge transfer from surroundings [41, 42]. This effect can influence the refractive index and reduce it as it results in the shift to the smaller dip wavelength. In our case, the appeared blue shift of the absorbance dip indicates that the SiO_2-NH_2@GO composite is aggregated due to Ep. Hence, a decrease in the resonance wavelength change is observed [see Fig. 6(b)]. For the sample with 12h deposition time, the evanescent wave vanished in the sensing layer, implying that the thickness is more than the up limitation of light mode absorption. Generally, as evident from Fig. 6, the location of the attenuation dip exhibits the maximum blue shift accompanied by a slight intensity increase using the probe fabricated in the optimal conditions (i.e., 0.01g GO, 5h SiO-NH@GO deposition time followed by 8h PDA coating). The variations of the real and the imaginary part of the effective RI (n_{eff}) caused by Ep concentration leads to absorption tunability, resulting in the resonance wavelength red- or blue- shift [43]. Herein, the blue shift could be attributed to the fact that as the Ep concentration increases, the real part of n_{eff} slightly decreases. This is confirmed by increasing the output transmitted intensity stem from the abundant hydroxyl and amino groups in PDA conjugating direct Ep target molecules.

In contrast, more absorbed light should be observed with an increase in the n_{eff} (i.e., decreased transmitted intensity due to increasing the Ep concentration). The peak of the n_{eff} imaginary part plays an essential role in the shift in direction [44]. Another probe with a higher concentration of GO and more deposition time of PDA is fabricated with a 5 h sol-gel step and 8h PDA polymerization time. The LMR spectra in Fig. 6(c) and 6(d) imply a sensing layer with a more significant absorbing feature [39]. So, the sensing performance reveals an apparent red-shift from 711 to 719 nm, accompanied by an intensity decrease. Sensor resolution signifies the most negligible variation in the sensing medium RI that generates a detectable change in the output signal [45]. The measurements show that the resolution of this sensor is 200nM.

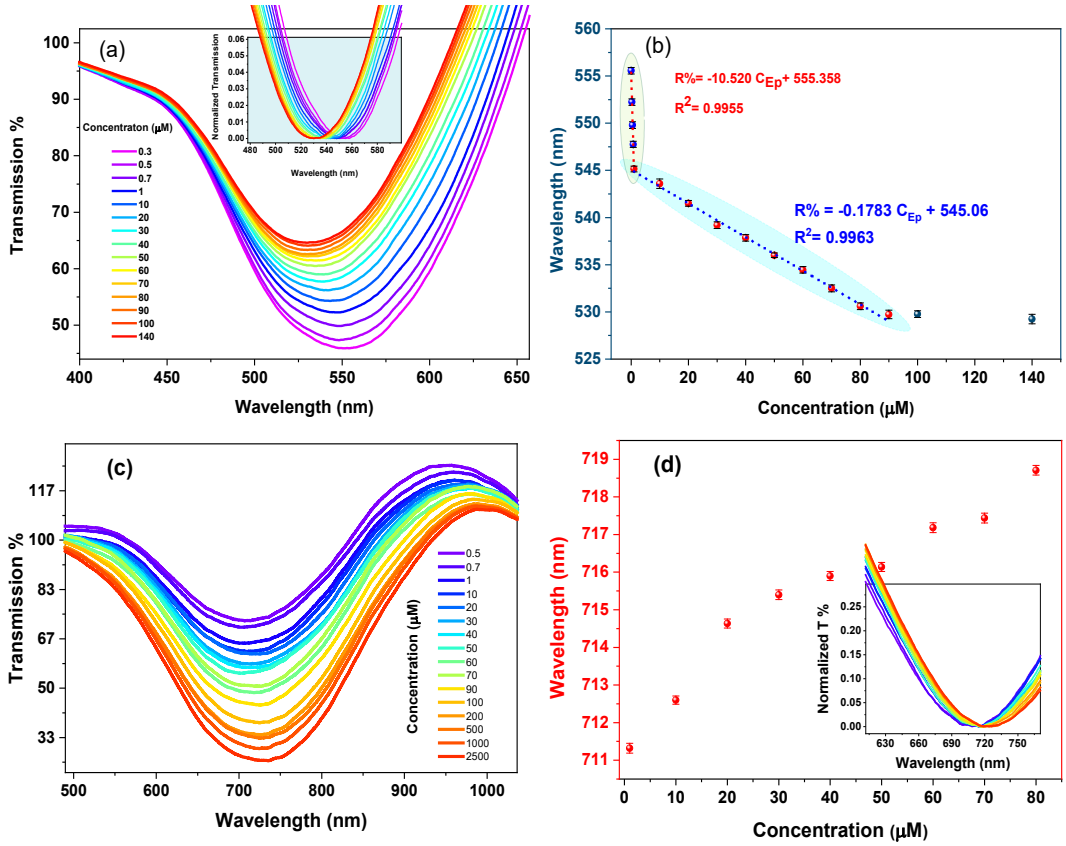

Fig.6: (a, c) LMR spectra and (b, d) variation of resonance wavelength with Ep concentration in 5h silane Sol-Gel step and 8h PDA polymerization, 0.01g and 0.1g GO, respectively.

When the particle size is smaller than the light wavelength, the Maxwell–Garnett model [46] can be used to calculate the dielectric function of the nano-composite. For two-component materials with dielectric constants, ε_1 (component 1, nano-particles) and ε_2 (component 2, dielectric host material), the effective dielectric function of the composite material (in our case, SiO_2-NH_2@GO) is calculated by the formula [47]:

$$\varepsilon_{\text{eff}} = \varepsilon_2 \frac{\varepsilon_1+2\varepsilon_2+2f(\varepsilon_1-\varepsilon_2)}{\varepsilon_1+2\varepsilon_2-f(\varepsilon_1-\varepsilon_2)} \qquad (1)$$

Here, f is the filling fraction of the first component (i.e., GO) into the second component (i.e., SiO_2), which is estimated from the volume incorporated into the solution. The attenuation dip is induced by multi-mode interference (MMI) for our coated optical fiber.

To further disclose the concrete absorbing sensing mechanism, the finite element method (FEM) with commercial software (COMSOL Multiphysics) is used to analyze the effective RI and electric field distribution of the guiding modes in the core region. The details of the simulation model and calculated parameters are introduced in our earlier work [48], as well as the structure specification reported in section S5.

In Fig. 7(a), the effective imaginary part of RI, $\mathrm{Im}(n_{\mathrm{eff}})$, of the 6 modes is plotted versus wavelength for the Ep-IPDA-coated multi-mode optical fiber. For the absorption-based optical sensors, a maximum magnitude of $\mathrm{Im}(n_{\mathrm{eff}})$ is needed for appearing attenuation loss, which corresponds to the LMR. The dip of $\mathrm{Im}(n_{\mathrm{eff}})$ around 560nm means that there will be an attenuation dip in the transmission spectrum, which is due to the LMR effect caused by the mode coupling between the Ep-IPDA and optical fiber. This finding is consistent with the previous experimental observations. To get an intuitive understanding of the LMR effect in the as-prepared coated layers, the electric field mode distributions in the core region at $\lambda = 560\mathrm{nm}$ are displayed in Fig. 7(b). It can be seen that the electric field distributions of the lossy modes in the vicinity of the coated layer result in the strongest coupling between the core guiding modes and leaky modes of the coated layer. In this situation, the phases match well, and the launched light maximally transits into the lossy mode immersed in the Ep-IPDA hybrid film.

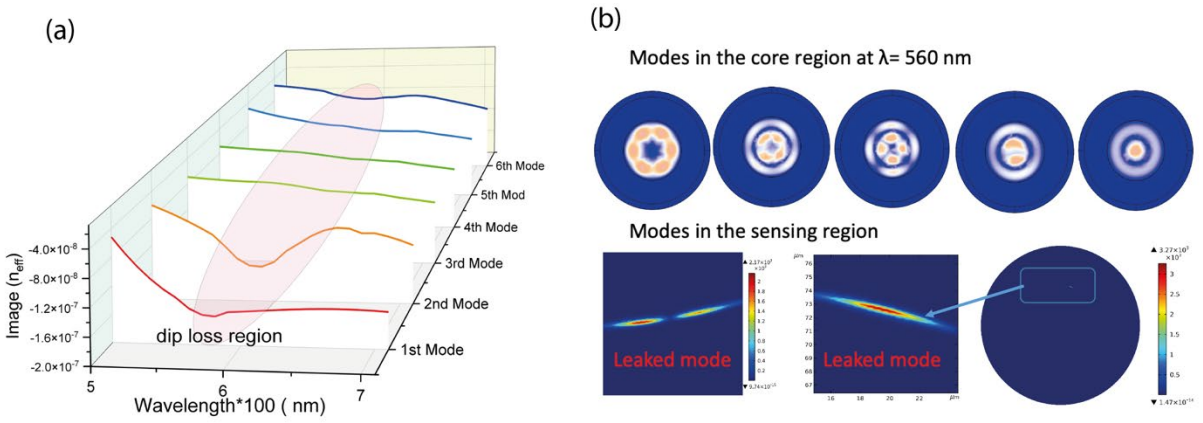

Fig. 7 (a) Imaginary part of effective RI of modes for the Ep-IPDA coated multi-mode optical fiber and (b) electric field distributions of the modes in the different region

Selectivity and Stability:

The selectivity of the Ep-IPDA LMR absorptive-based probes fabricated under optimal conditions is evaluated by analyzing Ep, DA, ascorbic acid, urea, and glucose. The effect of these interferes with a specific concentration of 50μM in the determination of Ep with a similar concentration is investigated, as shown in Fig. 8(a). This finding demonstrates that the molecular imprinting PDA provides good selectivity for Ep with common simultaneous interferents (the interferents impact is less than 5% for all solutions). The response of the Ep-IPDA sensor is nearly 5 times higher in magnitude than that of the non-imprinted polymer (NIP) probe sensor, indicating the highly sensitive recognition of the Ep-IPDA sensor.

The imprinting factor (*IF*) is evaluated by comparing the sensor response to the target under specific-to-nonspecific binding ($IF = R_{MIP}/R_{NIP}$) [49] as an essential parameter in evaluating the effectiveness of the imprinting process (see Fig. 8). The high *IF* values imply a very specific recognition of the target analyte, which can be mainly due to shape identification and electrostatic polymer structure. Fig. 8(b) shows the bar diagram representing the shift in peak absorbance wavelength for different concentration samples. It can be seen that Δλ of Ep is considerably higher than that of other molecules. These observations indicate that the binding sites and recognition caves of Ep existed within the film, which fit the target molecular structure.

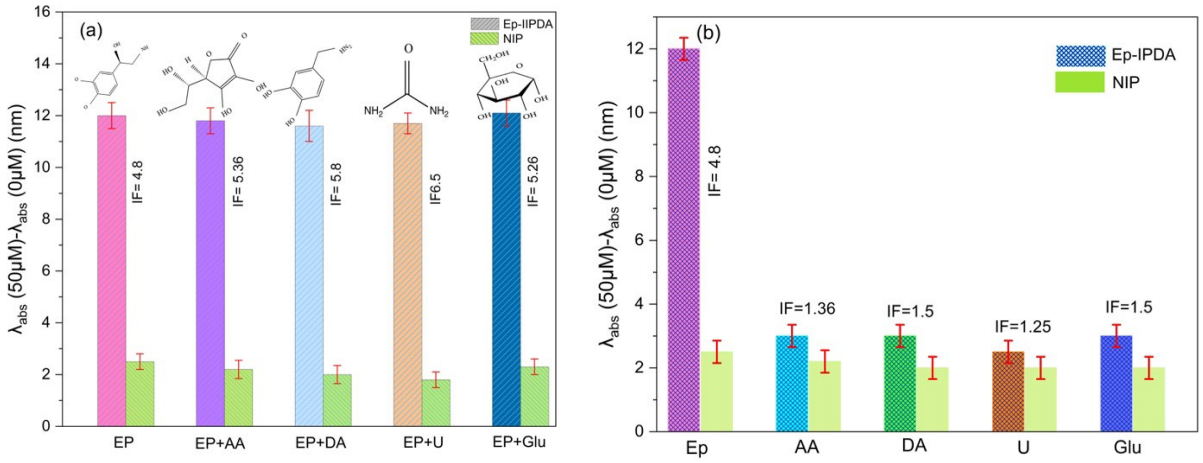

Fig. 8: (a, b) Selectivity plots of Ep-IPDA on the finalized probe.

The selective mechanism also can be attributed to the fact that the abundant hydroxyl and amino groups in PDA allow direct Ep conjugation, as shown in Fig. 9(a). Stability is a vital proficiency requirement for sensor applicability. To check the performance of the sensor, the probe is fixed into the flow cell. First, the sample without analyte is poured into the flow cell, and its intensity spectrum is recorded. After that, the 50µM sample is poured into the flow cell, and the intensity spectra are recorded. The sample solution is removed from the flow cell after a while. This process is repeated for three cycles. In Any measurement, the sample is allowed to remain in the probe vicinity. The recorded data are shown in Fig. 9(b), where a minor change in the intensity is found. The stability test is performed, and the sensor is observed to have acceptable stability.

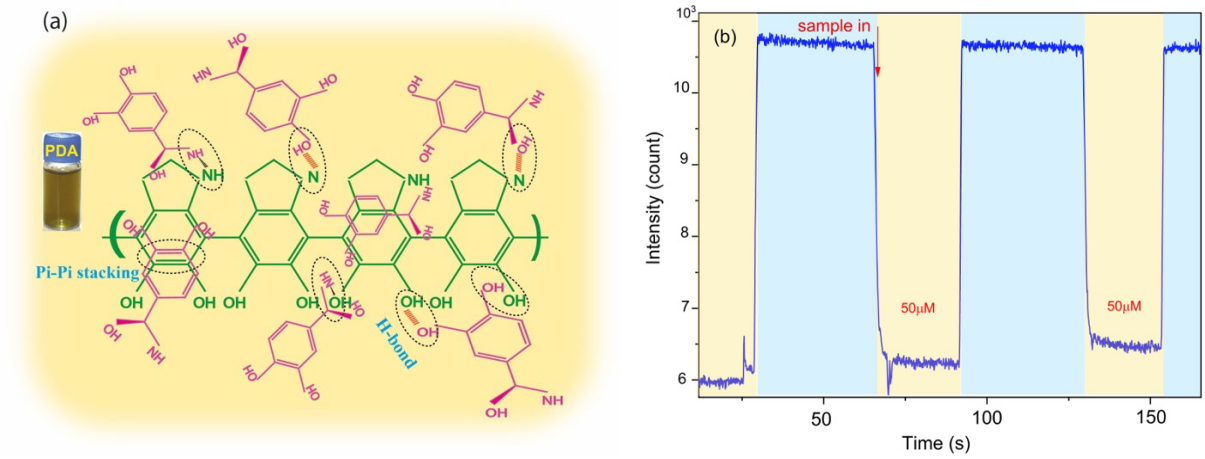

Fig. 9: (a) The sensing mechanism based on hydroxyl and amino groups in PDA allow Ep conjugation directly, (b) Stability plots of the probe prepared with Ep-IPDA layers over an unclad fiber core.

The obtained results are compared with previously reported sensing techniques and listed in Table 1. The present method is efficient as it has good linearity for Ep detection within a sufficiently wide range and a low LOD compared to the previously reported sensors.

Table 1: Comparison of various methods reported for Ep determination.

Method	Material	linear concentration range	LOD (Limit of detection)	Ref
Electrochemical	SnO_2-Graphene	0.5-200µM	0.017µM	[50]

Electrochemical	r-GO	0.001 µM to 1000 µM	0.0012 µM	[51]
Electrochemical	graphene nanoribbons	6.4×10^{-6} 1.0×10^{-4} M	2.1 µM	[52]
Electrochemical	ordered mesoporous carbon/nickel oxide	8.0×10^{-7} - 5.0×10^{-5} M	0.085 µM	[53]
Optical fiber biosensor	Ep-IPDA	0.3-90 µM	0.07µM	This work

Analysis of real samples:

To evaluate the workability of the proposed optical fiber sensor, the determination of Ep in injection solution and human urine samples are analyzed using the standard addition method. Ep hydrochloride injection samples (standard content of Ep 1mg.mL^{-1}; 1 mL per injection) are purchased from a local pharmacy. Human urine samples are obtained from a local pathology clinic. The real sample for the injection is diluted approximately to bring it to the working range concentration. Also, a standard stock solution of Ep equivalent to the real sample is prepared, as well as in human urine samples. The optical response of Ep in the real samples solutions is estimated by adding different concentrations of standard solution (i.e., Ep), listed in Table 2. Thus, the fabricated biosensors can effectively analyze Ep in pharmaceutical formulations and human urine samples.

Table 2: Studies of Ep sensing in human urine and injection samples.

Sample	Add (µM)	Found (µM)	Recovery %	RSD (% n=3)
EP injection (10µM)	30	40	100	0.58
	40	49.5	99	0.38
	50	59	98.33	0.2
Human urine	0	ND	-	
	30	29.5	98.33	0.81
	40	40	100	0.57
	50	51	102	0.68

4. Conclusion

A nano-composite absorptive optical probe of Ep-IPDA is successfully fabricated based on LMR phenomena to detect Ep. The combination of PDA, molecularly imprinted polymer, improved adsorption, selectivity, and SiO_2-NH_2@GO is exploited to provide the adhesion linkers besides providing the lossy conception of the sensing layer. The proposed sensor can measure target analytes at a low concentration with a LOD of 0.7 μM compared to other Ep sensors. The modified optical fiber shows a broad linear range and long-term stability. Hence, this optical sensor can be used successfully to determine Ep and introduce optical fiber substrate design as feasible and remote monitoring with required miniaturization for any bio-sensor applications. Additionally, these efficient achievements confirm the label-free diagnosis of Ep and open up a novel opportunity to quantitatively monitor biological molecules with a poor concentration in different aqueous matrices.

References:

[1] P. Shaikshavali *et al.*, "A simple sonochemical assisted synthesis of nanocomposite (ZnO/MWCNTs) for electrochemical sensing of Epinephrine in human serum and pharmaceutical formulation," vol. 584, p. 124038, 2020.

[2] X. Lu *et al.*, "A novel nanocomposites sensor for epinephrine detection in the presence of uric acids and ascorbic acids," vol. 56, no. 21, pp. 7261-7266, 2011.

[3] W. Dong *et al.*, "Synthesis of tetrahexahedral Au-Pd core–shell nanocrystals and reduction of graphene oxide for the electrochemical detection of epinephrine," vol. 512, pp. 812-818, 2018.

[4] N. G. Mphuthi, A. S. Adekunle, and E. E. J. S. r. Ebenso, "Electrocatalytic oxidation of Epinephrine and Norepinephrine at metal oxide doped phthalocyanine/MWCNT composite sensor," vol. 6, no. 1, pp. 1-20, 2016.

[5] S. Govindaraju, A. S. Reddy, J. Kim, and K. J. A. S. S. Yun, "Sensitive detection of epinephrine in human serum via fluorescence enhancement of gold nanoclusters," vol. 498, p. 143837, 2019.

[6] S. Wei, G. Song, and J.-M. J. J. o. C. a. Lin, "Separation and determination of norepinephrine, epinephrine and isoprinaline enantiomers by capillary electrophoresis in pharmaceutical formulation and human serum," vol. 1098, no. 1-2, pp. 166-171, 2005.

[7] Y. Zhang, B. Wang, H. Xiong, W. Wen, and N. J. M. J. Cheng, "A ratiometric fluorometric epinephrine and norepinephrine assay based on carbon dot and CdTe quantum dots nanocomposites," vol. 146, pp. 66-72, 2019.

[8] H. Qiu, C. Luo, M. Sun, F. Lu, L. Fan, and X. J. C. Li, "A chemiluminescence sensor for determination of epinephrine using graphene oxide–magnetite-molecularly imprinted polymers," vol. 50, no. 11, pp. 4052-4060, 2012.

[9] C. Ji, J. Walton, Y. Su, and M. J. A. c. a. Tella, "Simultaneous determination of plasma epinephrine and norepinephrine using an integrated strategy of a fully automated protein

precipitation technique, reductive ethylation labeling and UPLC–MS/MS," vol. 670, no. 1-2, pp. 84-91, 2010.
[10] N. Saraf, A. Bosak, A. Willenberg, S. Das, B. J. Willenberg, and S. J. R. a. Seal, "Colorimetric detection of epinephrine using an optimized paper-based aptasensor," vol. 7, no. 77, pp. 49133-49143, 2017.
[11] B. Kaur, R. J. S. Srivastava, and A. B. Chemical, "Simultaneous determination of epinephrine, paracetamol, and folic acid using transition metal ion-exchanged polyaniline–zeolite organic–inorganic hybrid materials," vol. 211, pp. 476-488, 2015.
[12] E. Wierzbicka, M. Szultka-Młyńska, B. Buszewski, G. D. J. S. Sulka, and A. B. Chemical, "Epinephrine sensing at nanostructured Au electrode and determination its oxidative metabolism," vol. 237, pp. 206-215, 2016.
[13] S. Fatma, B. B. Prasad, S. Jaiswal, R. Singh, K. J. B. Singh, and Bioelectronics, "Electrochemical simultaneous analysis of dopamine and epinephrine using double imprinted One MoNomer acryloylated graphene oxide-carbon black composite polymer," vol. 135, pp. 36-44, 2019.
[14] F. Liu and X. J. J. o. E. C. Kan, "Conductive imprinted electrochemical sensor for epinephrine sensitive detection and double recognition," vol. 836, pp. 182-189, 2019.
[15] J. d. D. Habimana, J. Ji, and X. J. A. L. Sun, "Minireview: trends in optical-based biosensors for point-of-care bacterial pathogen detection for food safety and clinical diagnostics," vol. 51, no. 18, pp. 2933-2966, 2018.
[16] H. Zhou, J. Liu, J.-J. Xu, S.-S. Zhang, and H.-Y. J. C. S. R. Chen, "Optical nano-biosensing interface via nucleic acid amplification strategy: construction and application," vol. 47, no. 6, pp. 1996-2019, 2018.
[17] N. Zhong *et al.*, "Monitoring Microalgal Biofilm Growth and Phenol Degradation with Fiber-Optic Sensors," vol. 91, no. 23, pp. 15155-15162, 2019.
[18] X.-d. Wang and O. S. J. A. c. Wolfbeis, "Fiber-optic chemical sensors and biosensors (2015–2019)," vol. 92, no. 1, pp. 397-430, 2019.
[19] F. Bertani *et al.*, "Optical detection of aflatoxins B in grained almonds using fluorescence spectroscopy and machine learning algorithms," vol. 112, p. 107073, 2020.
[20] J. K. Nayak, P. K. Maharana, and R. J. J. o. P. D. A. P. Jha, "Dielectric over-layer assisted graphene, its oxide and MoS2-based fibre optic sensor with high field enhancement," vol. 50, no. 40, p. 405112, 2017.
[21] A. M. Shrivastav, G. Sharma, R. J. B. Jha, and Bioelectronics, "Hypersensitive and selective biosensing based on microfiber interferometry and molecular imprinted nanoparticles," vol. 141, p. 111347, 2019.
[22] T. Batchman, G. M. J. I. T. o. M. T. McWright, and Techniques, "Mode coupling between dielectric and semiconductor planar waveguides," vol. 30, no. 4, pp. 628-634, 1982.
[23] F. Yang and J. J. J. o. M. O. Sambles, "Determination of the optical permittivity and thickness of absorbing films using long range modes," vol. 44, no. 6, pp. 1155-1163, 1997.
[24] I. Del Villar, C. R. Zamarreño, M. Hernaez, F. J. Arregui, and I. R. J. J. o. L. T. Matias, "Lossy mode resonance generation with indium-tin-oxide-coated optical fibers for sensing applications," vol. 28, no. 1, pp. 111-117, 2010.
[25] V. Torres Landívar, M. Beruete Díaz, P. Sánchez Zábal, and I. Del Villar, "Indium tin oxide refractometer in the visible and near infrared via lossy mode and surface plasmon

resonances with Kretschmann configuration," *Applied Physics Letters 108, 043507 (2016),* 2016.
[26] X.-Z. Wang and Q. Wang, "Theoretical analysis of a novel microstructure fiber sensor based on lossy mode resonance," *Electronics,* vol. 8, no. 5, p. 484, 2019.
[27] B. Cui, P. Liu, X. Liu, S. Liu, Z. J. J. o. M. R. Zhang, and Technology, "Molecularly imprinted polymers for electrochemical detection and analysis: Progress and perspectives," vol. 9, no. 6, pp. 12568-12584, 2020.
[28] W. Cheng *et al.*, "Versatile polydopamine platforms: synthesis and promising applications for surface modification and advanced nanomedicine," vol. 13, no. 8, pp. 8537-8565, 2019.
[29] J. Li *et al.*, "Polydopamine-assisted decoration of TiO2 nanotube arrays with enzyme to construct a novel photoelectrochemical sensing platform," vol. 255, pp. 133-139, 2018.
[30] B. Ramezanzadeh, E. Ghasemi, M. Mahdavian, E. Changizi, and M. M. J. C. E. J. Moghadam, "Characterization of covalently-grafted polyisocyanate chains onto graphene oxide for polyurethane composites with improved mechanical properties," vol. 281, pp. 869-883, 2015.
[31] W. Cheng *et al.*, "Versatile polydopamine platforms: synthesis and promising applications for surface modification and advanced nanomedicine," *Acs Nano,* vol. 13, no. 8, pp. 8537-8565, 2019.
[32] L. Kou and C. Gao, "Making silica nanoparticle-covered graphene oxide nanohybrids as general building blocks for large-area superhydrophilic coatings," *Nanoscale,* vol. 3, no. 2, pp. 519-528, 2011.
[33] B. Ramezanzadeh, E. Raeisi, and M. Mahdavian, "Studying various mixtures of 3-aminopropyltriethoxysilane (APS) and tetraethylorthosilicate (TEOS) silanes on the corrosion resistance of mild steel and adhesion properties of epoxy coating," *International Journal of Adhesion and Adhesives,* vol. 63, pp. 166-176, 2015.
[34] L. Liu, Y. Lei, Z. Zhang, J. Liu, S. Lv, and Z. Guo, "Fabrication of PDA@ SiO2@ rGO/PDMS dielectric elastomer composites with good electromechanical properties," *Reactive and Functional Polymers,* vol. 154, p. 104656, 2020.
[35] C. Y. Lee, J.-H. Bae, T.-Y. Kim, S.-H. Chang, and S. Y. Kim, "Using silane-functionalized graphene oxides for enhancing the interfacial bonding strength of carbon/epoxy composites," *Composites Part A: Applied Science and Manufacturing,* vol. 75, pp. 11-17, 2015.
[36] F. Wang *et al.*, "Construction of polydopamine/silver nanoparticles multilayer film for hydrogen peroxide detection," vol. 706, pp. 102-107, 2013.
[37] Á. Molnár, "Polydopamine–its Prolific Use as Catalyst and Support Material," *ChemCatChem,* vol. 12, no. 10, pp. 2649-2689, 2020.
[38] S. Haeri, B. Ramezanzadeh, and M. Asghari, "A novel fabrication of a high performance SiO2-graphene oxide (GO) nanohybrids: Characterization of thermal properties of epoxy nanocomposites filled with SiO2-GO nanohybrids," *Journal of colloid and interface science,* vol. 493, pp. 111-122, 2017.
[39] H. Zheng *et al.*, "Residual thickness enhanced core-removed D-shaped single-mode fiber and its application for VOC evaporation monitoring," *Optics Express,* vol. 28, no. 10, pp. 15641-15651, 2020.

[40] S. P. Usha, A. M. Shrivastav, and B. D. Gupta, "Semiconductor metal oxide/polymer based fiber optic lossy mode resonance sensors: A contemporary study," *Optical Fiber Technology,* vol. 45, pp. 146-166, 2018.
[41] C. Elosúa *et al.*, "Lossy mode resonance optical fiber sensor to detect organic vapors," *Sensors and Actuators B: Chemical,* vol. 187, pp. 65-71, 2013.
[42] S. P. Usha, A. M. Shrivastav, and B. D. Gupta, "Silver nanoparticle noduled ZnO nanowedge fetched novel FO-LMR based H2O2 biosensor: A twin regime sensor for in-vivo applications and H2O2 generation analysis from polyphenolic daily devouring beverages," *Sensors and Actuators B: Chemical,* vol. 241, pp. 129-145, 2017.
[43] I. Del Villar *et al.*, "Design rules for lossy mode resonance based sensors," *Applied optics,* vol. 51, no. 19, pp. 4298-4307, 2012.
[44] L. Dong *et al.*, "All-fiber multifunctional electrooptic prototype device with a graphene/PMMA (poly (methyl methacrylate)) hybrid film integrated on coreless side-polished fibers," *ACS Applied Electronic Materials,* vol. 2, no. 2, pp. 447-455, 2020.
[45] E. Wijaya *et al.*, "Surface plasmon resonance-based biosensors: From the development of different SPR structures to novel surface functionalization strategies," *Current Opinion in Solid State and Materials Science,* vol. 15, no. 5, pp. 208-224, 2011.
[46] R. Ruppin, "Evaluation of extended Maxwell-Garnett theories," *Optics communications,* vol. 182, no. 4-6, pp. 273-279, 2000.
[47] A. E. Lidiya, R. V. J. Raja, Q. M. Ngo, and D. Vigneswaran, "Detecting hemoglobin content blood glucose using surface plasmon resonance in D-shaped photonic crystal fiber," *Optical Fiber Technology,* vol. 50, pp. 132-138, 2019.
[48] Z. Heidarnia, H. Khoshsima, R. Parvizi, and H. Heidari, "Comprehensive investigation on chalcogenide thin film coated multimode optical fiber: Visible evanescent-wave absorption refractometer," *Journal of Non-Crystalline Solids,* vol. 586, p. 121567, 2022.
[49] T. Azargoshasb, H. A. Navid, R. Parvizi, and H. Heidari, "Evanescent wave optical trapping and sensing on polymer optical fibers for ultra-trace detection of glucose," *ACS omega,* vol. 5, no. 35, pp. 22046-22056, 2020.
[50] N. Lavanya *et al.*, "Simultaneous electrochemical determination of epinephrine and uric acid in the presence of ascorbic acid using SnO2/graphene nanocomposite modified glassy carbon electrode," *Sensors and Actuators B: Chemical,* vol. 221, pp. 1412-1422, 2015.
[51] W. Dong *et al.*, "Synthesis of tetrahexahedral Au-Pd core–shell nanocrystals and reduction of graphene oxide for the electrochemical detection of epinephrine," *Journal of colloid and interface science,* vol. 512, pp. 812-818, 2018.
[52] R. Sainz *et al.*, "Chemically synthesized chevron-like graphene nanoribbons for electrochemical sensors development: determination of epinephrine," *Scientific reports,* vol. 10, no. 1, pp. 1-11, 2020.
[53] X. Yang *et al.*, "Selective determination of epinephrine using electrochemical sensor based on ordered mesoporous carbon/nickel oxide nanocomposite," *Talanta,* p. 122545, 2021.